



## On local strength of a spherical vessel with pits distributed along the equator

Daria D. Okulova, Liana A. Almazova, Olga S. Sedova, Yulia G. Pronina

*Saint Petersburg State University, St. Petersburg State University, 7/9 Universitetskaya nab., St. Petersburg, 199034 Russia*

*st062247@student.spbu.ru, <http://orcid.org/0000-0001-2345-6789>*

*st080595@student.spbu.ru, <https://orcid.org/0000-0001-8695-3598>*

*o.s.sedova@spbu.ru, <https://orcid.org/0000-0001-9097-8501>*

*y.pronina@spbu.ru, <https://orcid.org/0000-0003-4978-6238>*

**ABSTRACT.** The effect of multiple shallow corrosion pits on the strength of a spherical vessel subjected to internal pressure is studied. The pits are considered both randomly and evenly distributed along the equator on the outer surface of the vessel. The dependencies of the stress concentration factor on the number of the pits are compared for linearly elastic and elastic-plastic material with hardening. The behavior of the vessels made of elastic and elastoplastic materials turns out to be qualitatively different. The approximation of periodic pits arrangement is discussed.

**KEYWORDS.** Pitting corrosion, Surface defects, Spherical shell, Pressure vessel.



**Citation:** Okulova, D., Almazova, L., Sedova, O., Pronina, Y., On local strength of a spherical vessel with pits distributed along the equator, *Frattura ed Integrità Strutturale*, 63 (2023) 80-90.

**Received:** 31.05.2022

**Accepted:** 04.10.2022

**Online first:** 29.10.2022

**Published:** 01.01.2023

**Copyright:** © 2023 This is an open access article under the terms of the CC-BY 4.0, which permits unrestricted use, distribution, and reproduction in any medium, provided the original author and source are credited.

### INTRODUCTION

Pressure vessels are common devices for various industrial applications [1-4]. The most preferred vessel shape to hold internal pressure is spherical [5]. Moreover, temperature conditions of the environment have the least effect on the contents of the spherical vessel due to the smallest surface area per unit volume. Pressure vessels are usually exploited in aggressive environments that may result in general or local corrosion of their parts. General mechanochemical corrosion of elastic or elastic-plastic thin- and thick-walled spherical vessels was modeled, e.g., in the works [6-10].

Pitting corrosion may be initiated by a local damage of a protective coating or an oxide film (which also may possess protective properties), as well as by many other factors which lead to chemical or physical heterogeneity at the metal surface [11, 12]. In natural conditions the likelihood of pitting corrosion is higher compared to uniform corrosion [13]. Despite having minor metal loss, the structures subjected to localized corrosion have significantly reduced service life.

Once appeared, local damages cause stress concentration in their adjacency. This may result in crack nucleation, and, consequently, the premature failure of a structural component. Therefore, assessment of the stress level in structural

elements with corrosion defects is an important issue to prevent the abrupt failure of the structures in an aggressive environment.

Shallow corrosion pits may show a spherical cap morphology with a constant pit depth/diameter ratio [14, 15]. Corrosion pits may also have more complex geometry [16-18]. However, most researchers used either simplification of pit forms or local thinning of structural elements [19-21]. Corrosion pits are usually idealized as conical [19], semi-elliptical [22-24], circular [18, 25-27], cylindrical [26, 28-30], and rounded rectangular shapes [31, 32]. Authors of [26, 27, 33] showed that the form of the defects (circular, conical, elliptical or cylindrical) has a slight effect on the ultimate strength of plates under different loading.

Stress fields around defects in structural elements are often analyzed using finite element method [34-37]. There are a number of papers focused on the effect of a single surface pitting on the service life of structural components. Stress distribution in the spherical shell with a single corrosion defect was addressed in [22, 38]. Many authors considered structures weakened by multiple surface defects. However, most of these studies focused on pipes [29, 39], plates [21, 27, 30, 40, 41], and shells [42-45].

Sedova [46] studied a spherical vessel with multiple defects uniformly located on its inner equator. The numerical simulations have shown that the maximum stresses in the vicinity of defects increase with the growing number of defects within a certain range, but further increase in the number of defects leads to a slight decrease in the stress values. Similar qualitative results were obtained in Liao, et. al. [39] using the Ramberg-Osgood plasticity model: the interaction between defects enhances with decreasing distance up to a certain limit when defects become close to intersection, while further decrease in spacing between defects provides the reduction of the interaction between defects.

In [29], it is shown that the effect of multiple surface defects on the strength of structures depends on the distribution pattern of pitting corrosion. Since in reality, the defects appear randomly, it is reasonable to use random patterns when modeling multiple pits on the surface of structural components. The influence of pittings randomly distributed over a small area of the surface of a sphere on the collapse pressure was analyzed in [47, 48]. Authors of [28] showed that the outer defect is more harmful to the pressure vessel than the inner one. A linearly elastic spherical vessel with several notches evenly distributed along its equator, subjected to internal pressure was considered in [49].

The present paper is devoted to the stress analysis of a spherical vessel under internal pressure, weakened by multiple shallow pits located along the equator on its outer surface. Results are compared for the bilinear plasticity hardening model and the linearly elastic model of the vessel material. Different numbers of defects with random arrangement and periodic arrangement are considered. The limiting case of toroidal notch is also studied.

## DESCRIPTION OF THE PROBLEM

A spherical vessel with multiple shallow pits along the equator on its outer surface is under study. Let  $r$  and  $R$  be the inner and outer radii of the vessel. All the pits have a spherical cap shape of the same size with curvature radius  $\delta$  and depth  $h = \delta/2$  (Fig. 1). A pseudo-random arrangement of the defects along the equator of the sphere and their different numbers  $n$  are considered. Along with separate notches, the “limiting” case of notches configuration is analyzed. This case corresponds to the complete covering of the equator of the sphere with a continuous toroidal notch with the same minimal curvature radius  $\delta$  and depth  $b$  (Fig. 2, the surface of the notch is highlighted with another color).

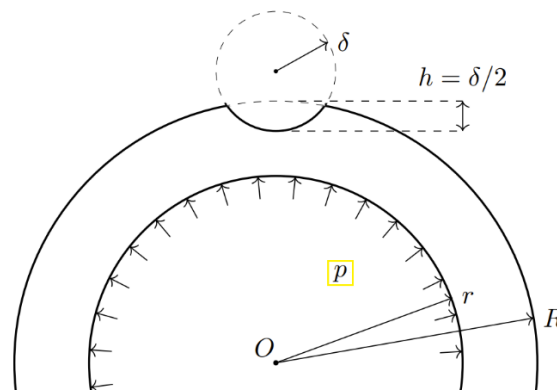


Figure 1: Central cross-section of the vessel with one surface defect.

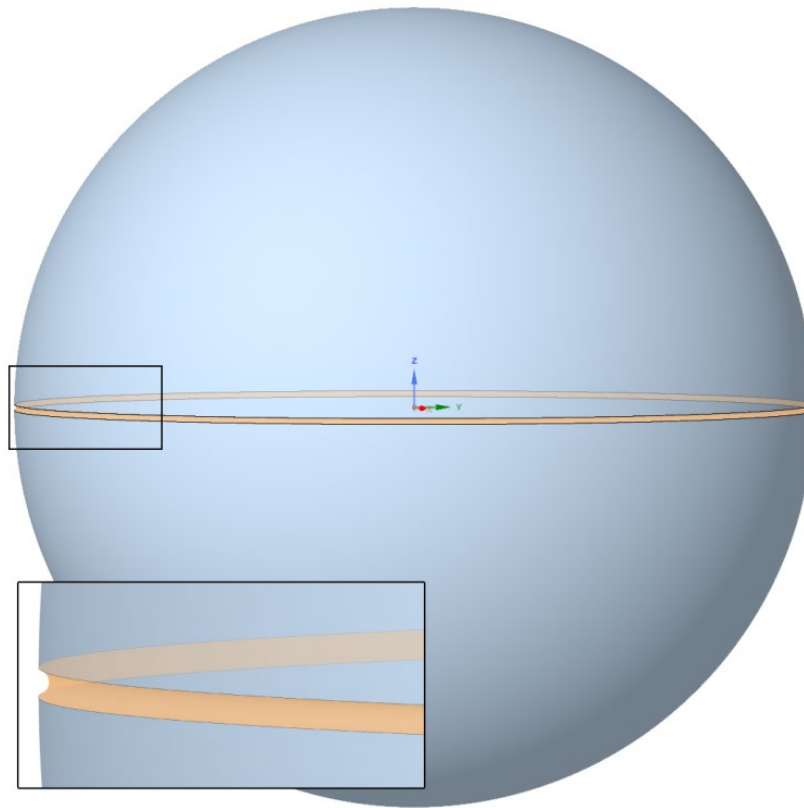


Figure 2: A sphere with a toroidal notch along the equator.

Pressure  $p$  is applied to the inner surface of the vessel. The problem is studied both within the framework of linearly elastic and bilinear elastic-plastic models.

For example, 304 stainless steel is chosen as the vessel material. The inner and outer radii of the sphere are  $r = 340$  mm and  $R = 350$  mm, respectively. The notches' curvature radius is  $\delta = 6$  mm, and the notch depth is  $h = 3$  mm. The number of the defects,  $n$ , varies from 2 to 260; additional geometries with  $n$  up to 320 are considered for the case of uniformly (periodically) located notches. Note that numbers  $n > 212$  correspond to the complete covering of the equator by the defects (their intersection), in the case of their periodical distribution.

## NUMERICAL ANALYSIS

To perform the finite element analysis, an array of 3D CAD-models of different geometries was built in ANSYS SpaceClaim. Each of the models represents the hollow sphere with the notches. Since the probability of the defects is supposed to be the same at every point on the equator, the uniform probability distribution was accepted. In order to create the random patterns of the defects along the equator of the vessel, the Python-function «random()» was used. Since the model of the sphere with the notches located on the equator is symmetric, only a half of the sphere was built as a CAD-model. The boundary condition on the face of symmetry was set to “Frictionless support” which prevents moving or deforming in the normal direction.

For mesh generation a ten-node tetrahedral element SOLID187 was utilized. In order to enhance the accuracy of the solution, the finite element mesh was refined in the vicinity of the defects.

The geometrical model with the continuous torus-shaped notch on the equator is axisymmetric; therefore, the cross section of the geometry was built in ANSYS DesignModeler. Before performing axisymmetric analysis for the geometry with the toroidal notch, special meshing methods with mesh refinement settings were set in the vicinity of the notch to achieve sufficient mesh quality. Fig. 3 shows mesh element quality on the fragment of the geometrical model capturing the vicinity of the notch.

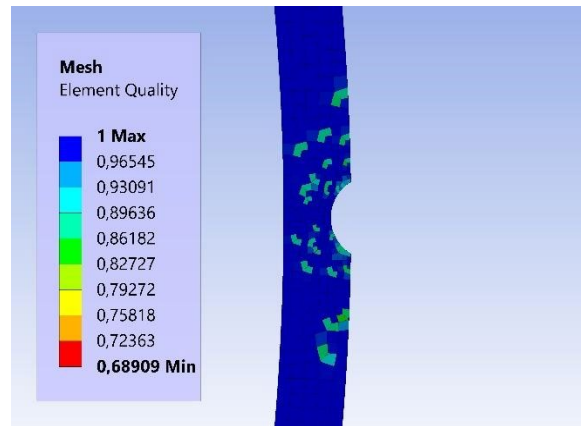


Figure 3: Mesh element quality in the vicinity of the toroidal notch.

The following data on material properties for 304 stainless steel are used: Young's modulus  $E = 185$  GPa, Poisson's ratio  $\nu = 0.27$ , yield strength  $\sigma_T = 210$  MPa and tangent modulus  $T = 1.16$  GPa.

For linearly elastic analysis, the material is assumed to behave according to Hooke's Law with the elastic constants given above. Internal pressure is set to  $p = 1$  MPa to stay in the framework of the elastic problem.

For elastic-plastic analysis, the bilinear plasticity model "Bilinear Isotropic Hardening" available in ANSYS Workbench material properties library is used. The vessel is subjected to internal pressure  $p = 6$  MPa which causes the plastic deformations of the material in the vicinity of the pits.

3D CAD-models are meshed using "Sizing" meshing options. The mesh is more refined at the weakened region and a smooth transition to a coarser mesh in regions far from notches is implemented. To ensure the convergence of the solution (its sensitivity to the mesh parameters), multiple calculations with different sizes of elements are carried out for each CAD-model. As a result, sizes of elements on the face of symmetry are set to 1.6 mm, while the sizes on the surface of notches are 0.5 mm. The estimated error value is about 2%.

For bilinear plasticity hardening model, about 30 iterations were needed for each geometry model to reach the convergence of the nonlinear solution.

Since linearly elastic and elastic-plastic analyses are performed with the same geometries and mesh parameters, there is no need to run two standalone calculations for each set of material properties. Two linked projects that share geometries and mesh parameters are used instead.

## RESULTS AND DISCUSSION

The maximum principal stress in the notched vessel was analyzed for various  $n$  from 2 to 260, and five different random distributions of pits for each  $n$  being considered. Let the maximum value of this stress for a certain geometry be denoted by  $\sigma_{max}$ .

It was observed that for the configurations where all the defects were either far enough from each other or, conversely, their centers were exceedingly close to each other (resulting in their extensive overlapping so that there were no thin ligaments between them), the maximum stress values were reached at the bottom of a certain pit or pits (Fig. 4). Concerning the configurations where the pits slightly overlap or close to overlapping, the maximum stress values were observed at the cusps formed by the adjacent boundaries (Fig. 5). This observation is in accordance with the results of [36, 39, 46]. For the toroidal notch, the maximum stress value was observed along the bottom of the notch (Fig. 6).

Let the stress concentration factor (one of all the possible factors) be denoted by  $K$ :

$$K = \frac{\sigma_{max}}{\sigma_{ideal}} \quad (1)$$

where  $\sigma_{ideal}$  is the maximum principal stress on the outer surface of an ideal shell (without defects) of the same size and under the same pressure:



$$\sigma_{ideal} = \frac{3p}{2(R^3 / r^3 - 1)} \quad (2)$$

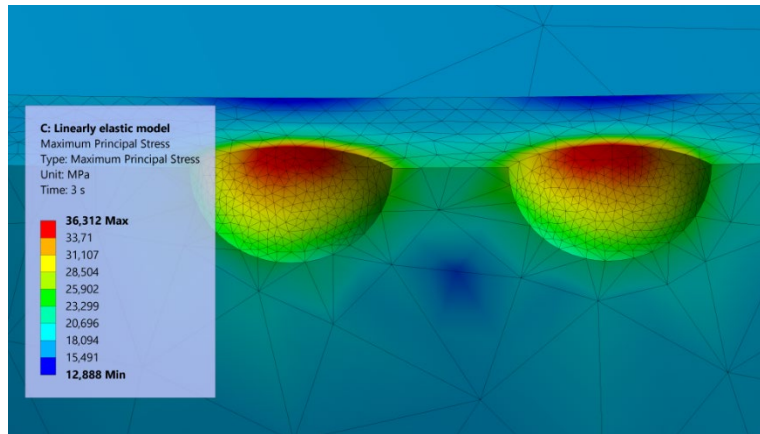


Figure 4: Stress distribution in the vicinity of pits sufficiently remote from each other (the plane of symmetry is horizontal). Linearly elastic model.

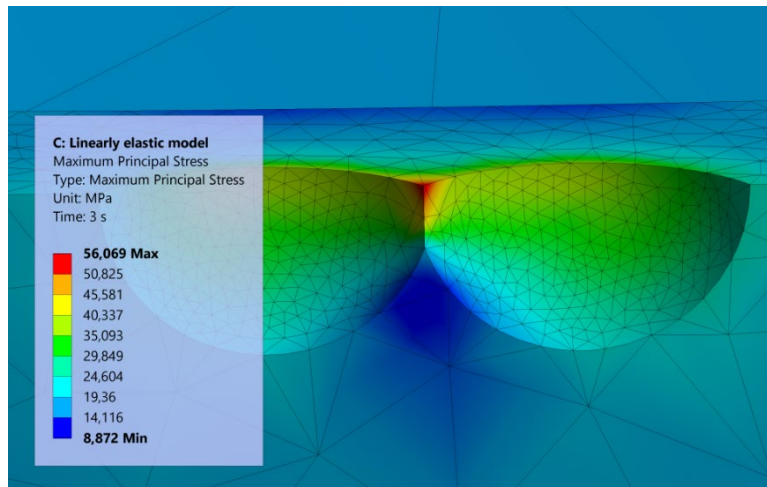


Figure 5: Stress distribution in the vicinity of overlapping pits (the plane of symmetry is horizontal). Linearly elastic model.

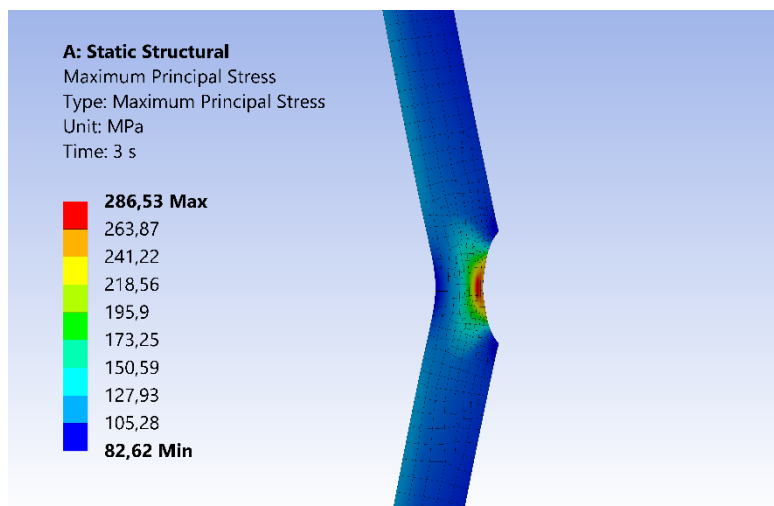


Figure 6: Stress distribution along the cross section of the vessel with a continuous toroidal notch. Elastic-plastic model.



In our cases,  $\sigma_{ideal} \approx 16.51$  MPa for  $p = 1$  MPa used in linear analysis and  $\sigma_{ideal} \approx 99.06$  MPa for  $p = 6$  MPa used in nonlinear analysis. Both of these values do not exceed the yield strength; therefore, no plastic deformation occurs on the surface of the ideal sphere for both the considered values of internal pressure.

Figs. 7 and 8 show the values of  $K$  for different random distributions of notches and for various numbers  $n$  within the frame-work of the linearly elastic (Fig. 7) and elastic-plastic (Fig. 8) models. Points of different colors for each  $n$  correspond to different random distributions of the pits. Dashed lines in the figures show the values of the stress concentration factor,  $K$ , in the sphere with the toroidal notch.

As can be seen from these figures, interaction of multiple defects may result in the significant increase in the maximum stresses with  $n$  increasing. The dependencies of  $K$  on  $n$  in the considered interval are qualitatively the same for both the models: at the beginning of the graphs, the values of  $K$  rise steeply and then a certain plateau (with a weak minimum inside) is formed at  $n > 200$ . The observed plateau may be explained by the overlaps of neighboring pits for large  $n$ . Obviously, the frequency of such overlaps grows with an increase in the number of the defects. However, the increase in  $K$  for the material in the elastic state is much higher than in the elastic-plastic: the value of  $K$  in the elastic sphere with multiple defects can be more than two times higher than that for a single defect, while in the elastic-plastic sphere the increase does not exceed 30%.

At first glance, it may seem strange that the maximum stresses in the elastic sphere with multiple pits may be larger than in the sphere with the toroidal notch (what is observed for  $n \geq 32$  in our case), while for the elastoplastic sphere the situation is opposite. Such behavior of the elastic sphere with multiple pits may be explained by the fact that the maximum stresses are observed at beak-like bridges between closely spaced defects (Fig. 5), which are absent in the sphere with a toroidal notch. The higher stresses at the bottom of the toroidal notch in the elastic-plastic vessel – compared to the stresses in the vicinity of the pits – are explained by the following reasoning. In the vessel with the continuous girdle notch, the vessel wall bends along the notch (see Fig. 6). Moreover, it is obvious that the bending deformations in the elastoplastic vessel are greater than in the elastic one, however, stresses in the last are not limited. Large deformations in the elastoplastic vessel initiate a hardening effect, resulting in an increase in stresses along the equatorial notch. In the vessel with separate random pits, such large bending deformations (which can lead to a hardening effect) do not occur. Therefore, stresses in the vicinity of individual pits in the elastoplastic vessel are smaller, since limited by a lower yield strength.

Moreover, it is expected that as the number of pits increases, the stresses in the vicinity of the pits should tend to the stresses in the vicinity of the torus. It is really true and confirmed by Figs. 9 and 10. These figures show the values of  $K$  for the elastic and elastic-plastic vessels with multiple uniformly (i.e. periodically) located pits.

As can be seen from Fig. 9, for the elastic material, the value of  $K$  experiences a sharp increase when thin ligaments or cusps form between adjacent pits (numbers  $n > 212$  correspond to pit overlapping). Starting from a certain number  $n$  (in Figs. 9 the peak is reached at  $n = 228$ ), cusps between the pits in the elastic vessel become more obtuse resulting in the gradual decrease in the maximum stresses approaching to the value corresponding to the toroidal notch.

Numerical experiments with other pit sizes lead to qualitatively the same dependencies of maximum stress values on the number of notches,  $n$ : for relatively small numbers of notches, the maximum stress grows slightly with growing  $n$ ; then (when thin ligaments form between adjacent pits) a sharp increase in the maximum stress is observed; as  $n$  grows further, the maximum stress slightly decreases. The results in Fig. 9 are consistent with ones obtained in [50] for linearly elastic sphere with multiple uniformly located pits with different values of notches sizes (both for  $\delta < 6$  mm and  $\delta > 6$  mm).

Fig. 10 demonstrates a nearly S-shaped dependency of  $K$  on  $n$  in the elastic-plastic vessel. A small jump in the value of  $K$  at  $n = 276$  is explained by the formation of a relatively smooth notch along the equator of the vessel and its bending, resulting in large deformations and hardening effect. For  $n > 275$ , the difference between the values of  $K$  for multiple defects and for torus is less than 3.5%.

Thus, Figs. 9 and 10 confirm that the maximum stresses in the vessel with multiple pits periodically distributed along the equator, tend to that for the toroidal notch. It is obvious that this tendency should be preserved for randomly located defects. Nevertheless, there is a difference in the behavior of dependencies  $K(n)$  for random and periodical distribution of the defects. The values of  $K$  for the random defects rise significantly faster than for the periodical pits, due to the random formation of dangerous cusps at various and even very small  $n$ . The same effect for large  $n$  also leads to the slower decrease in  $K$  values for random pits in the elastic sphere.

The difference between the peak value of  $K$  in Fig. 9 ( $K = 4.399$  at  $n = 228$ ) and the maximum values observed in Fig. 7 (which are greater than 4.5 for large  $n$ ) is explained by the fact that for periodically distributed pits, the cusp angle changes stepwise (since the distance between the pits changes stepwise as  $L/n - d$ , where  $L$  is the length of the sphere equator and  $d$  is the pit diameter) and the angle values corresponding to the maximum  $K$  observed in Fig. 9 are just skipped. For certain ratios  $d/L$  at a certain  $n$ , the distance between the neighboring pits can become very close to that which corresponds to the maximum possible value of  $K$ , then the maximum values of  $K$  for periodical pits will become closer to that for random pits.

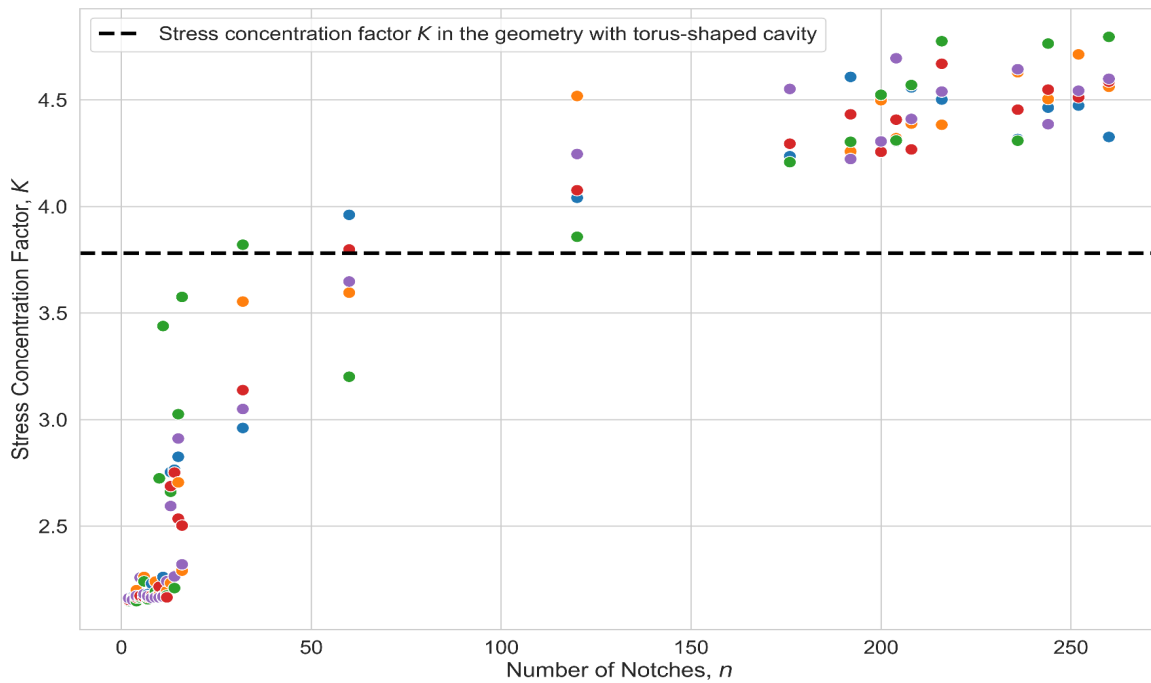


Figure 7: Stress concentration factor,  $K$ , in the shell with  $n$  randomly distributed defects (points) and with the toroidal notch (dashed line). Linearly elastic model.

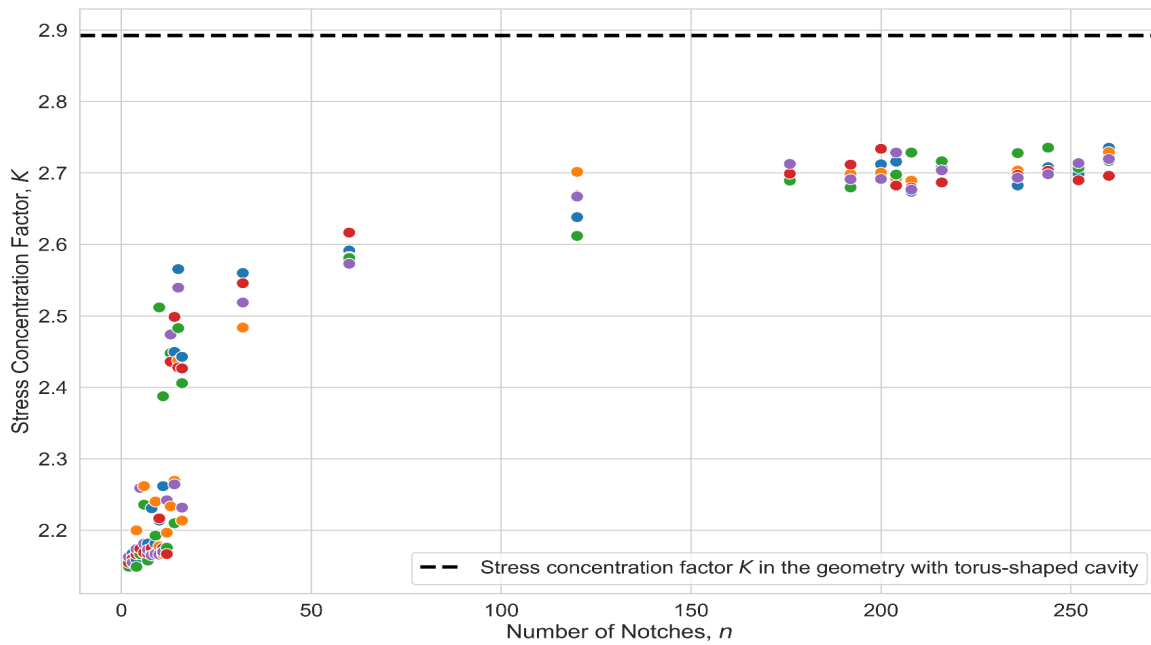


Figure 8: Stress concentration factor,  $K$ , in the shell with  $n$  randomly distributed defects (points) and with the toroidal notch (dashed line). Elastic-plastic model.

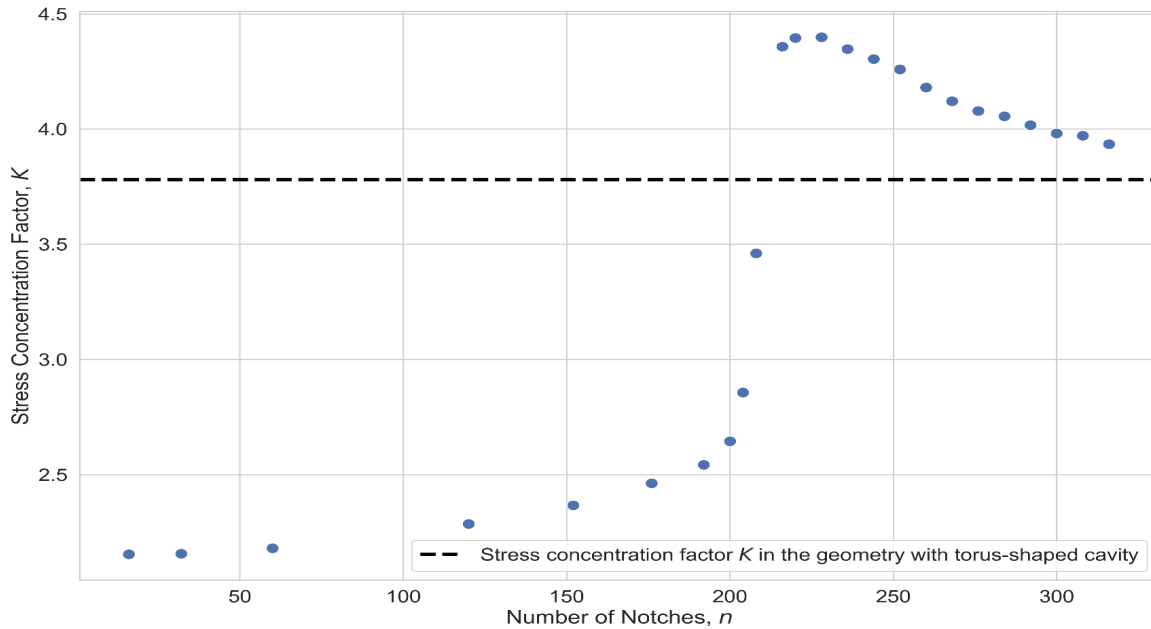


Figure 9: Stress concentration factor  $K$  in the shell with  $n$  defects uniformly located along the equator. Linearly elastic model.

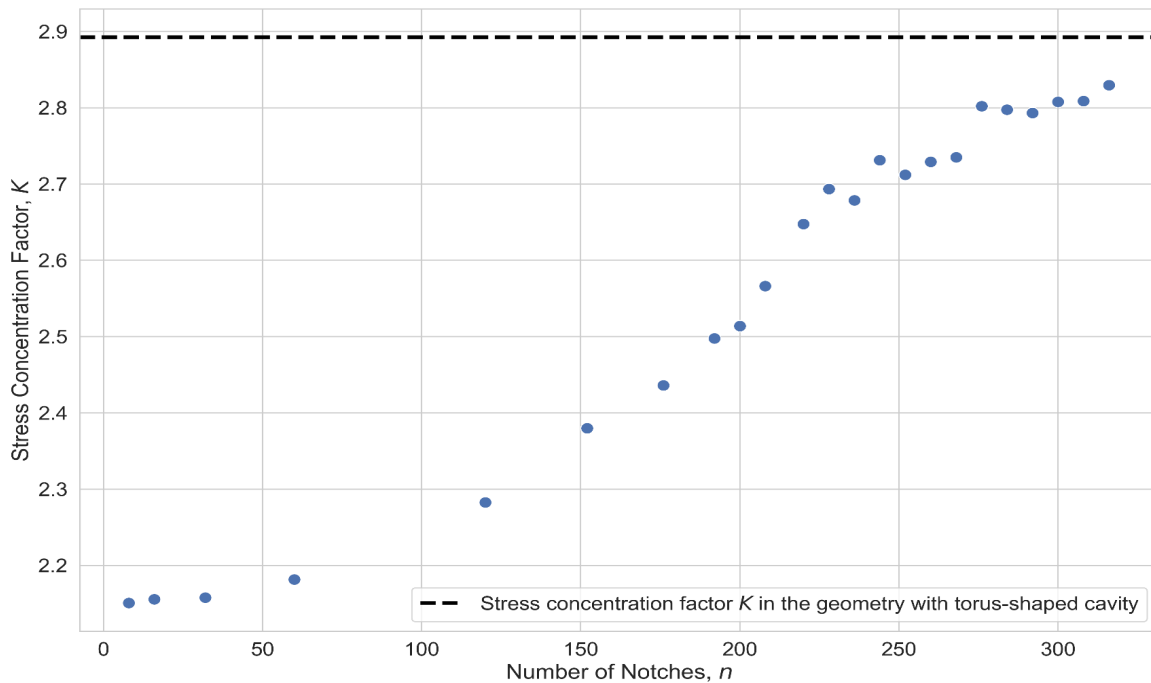


Figure 10: Stress concentration factor  $K$  in the shell with  $n$  defects uniformly located along the equator. Elastic-plastic model.

The opposite effect is observed for elastoplastic material: maximum values of  $K$  for randomly located pits (Fig. 8) are less than for periodical pits (Fig. 10). This is explained by the fact that at large  $n$  (starting from  $n=276$ ), multiple periodic pits form a relatively deep girdle notch, along which the wall of the sphere bends (almost the same as in the sphere with the



toroidal notch, see Fig. 6), resulting in a hardening effect and an increase in stresses. Randomly located pits do not form a continuous notch (as there may be relatively large gaps between the pits at random locations) where large bending deformations may occur. Therefore, the hardening effect does not manifest itself as noticeably as in a sphere with periodic pits.

Thus, the mutual arrangement of defects on the vessel surface may have a greater effect on its local strength than the total volume of metal loss.

## CONCLUSIONS

**B**ased on the study, the following common conclusions can be drawn:  
Interaction of multiple defects on the vessel surface may result in the significant increase in the maximum stresses with the number  $n$  of the defects increasing. However, behavior of the vessels with multiple defects is markedly different for linearly elastic and elastic-plastic models. First, it was observed that for the considered data, the value of maximum stresses in the elastic sphere with multiple defects can be more than two times higher than for a single defect, while in the elastic-plastic sphere this increase does not exceed 30%. Moreover, smoothing the surface due to the damage accumulation may lead to a little decrease in the stress concentration for elastic materials. Note that for other parameters, behavior of the vessels weakened by multiple pits was qualitatively the same.

The maximum stresses in the vessel with multiple pits located along the equator tend to that for the toroidal notch, as  $n$  increases. However, the maximum stresses in the elastic vessel with multiple pits may be significantly higher than that for the toroidal notch. This means that it is unacceptable to calculate the strength of elastic vessels with individual defects by considering vessels with a thickness smoothly reduced along a certain area. At the same time, for an elastic-plastic material, the maximum stresses in the vessel with a toroidal notch is the upper limit for the stresses in the vessel with multiple defects; therefore, for the strength analysis of the latter, the vessels with a smoothly reduced thickness can be considered.

Stress concentration in the vessels with randomly distributed defects can be much higher than in the vessel with the same number of periodical defects, due to the random formation of thin ligaments or sharp cusps between the adjacent defects. However, for elastoplastic vessels with large numbers of defects, the opposite phenomenon may be initiated by the hardening effect. This means that the mutual arrangement of defects on the vessel surface may have a greater effect on its local strength than the total volume of metal loss and that periodic solutions do not always provide good approximations for random defects.

## ACKNOWLEDGEMENTS

**T**his work was supported by the Russian Science Foundation, grant No 21-19-00100.

## REFERENCES

- [1] Li, K., Zheng, J., Zhang, Z., Gu, C., Zhang, X., Liu, S., Ge, H., Gu, G. and Lin, G. (2017). Experimental Investigation on Buckling of Ellipsoidal Head of Steel Nuclear Containment, *J. Press. Vess.-T. ASME*, 139(6), 061206. DOI: 10.1115/1.4038013.
- [2] Dehrouyeh-Semnani, A.M., Dehdashti, E., Yazdi, M.R.H. and Nikkhah-Bahrami, M. (2019). Nonlinear thermo-resonant behavior of fluid-conveying FG pipes, *Int. J. Eng. Sci.*, 144, 103141. DOI: 10.1016/j.ijengsci.2019.103141.
- [3] Dastjerdi, S., Akgöz, B., Civalek, Ö., Malikan, M. and Eremeyev, V.A. (2020). On the Non-linear Dynamics of Torus-shaped and Cylindrical Shell Structures, *Int. J. Eng. Sci.*, 156, 103371. DOI: 10.1016/j.ijengsci.2020.103371.
- [4] Karimihaghighi, R., Naghizadeh, M. and Javadpour, S. (2022). FFS Master Software For Fitness-For-Service Assessment of Hydrogen Induced Cracking Equipment Based on API 579-1/ASME FFS-1, *Frattura ed Integrità Strutturale*, 60, pp. 187–212. DOI: 10.3221/IGF-ESIS.60.14.
- [5] Nilsen, K. (2011). Development of low pressure filter testing vessel and analysis of electrospun nanofiber membranes for water treatment. Master's degree thesis, Wichita State University.



- [6] Pronina, Y.G. (2013). Lifetime assessment for an ideal elastoplastic thick-walled spherical member under general mechanochemical corrosion conditions, In: COMPLAS XII: Proceedings of the XII International Conference on Computational Plasticity: Fundamentals and Applications, CIMNE, pp. 729–738.
- [7] Gutman, E.M., Bergman, R.M. and Levitsky, S.P. (2016). Influence of internal uniform corrosion on stability loss of a thin-walled spherical shell subjected to external pressure, *Corros. Sci.*, 111, pp. 212–215. DOI: 10.1016/j.corsci.2016.04.018.
- [8] Pronina, Y., Sedova, O., Grekov, M. and Sergeeva, T. (2018). On corrosion of a thin-walled spherical vessel under pressure, *Int. J. Eng. Sci.*, 130, pp. 115–128. DOI: 10.1016/j.ijengsci.2018.05.004.
- [9] Pronina, Y. and Sedova, O. (2021). Analytical solution for the lifetime of a spherical shell of arbitrary thickness under the pressure of corrosive environments: The effect of thermal and elastic stresses, *J. Appl. Mech.-T. ASME*, 88, 061004. DOI: 10.1115/1.4050280.
- [10] Sedova, O. and Pronina, Y. (2022). The thermoelasticity problem for pressure vessels with protective coatings, operating under conditions of mechanochemical corrosion, *Int. J. Eng. Sci.*, 170, 103589. DOI: 10.1016/j.ijengsci.2021.103589.
- [11] Groysman, A. (2017). Physicochemical basics of corrosion at refineries units, *Top. Saf. Reliab. Qual.*, 32, pp. 17–36. DOI: 10.1007/978-3-319-45256-2\_3.
- [12] Liu, C., Li, X., Revilla, R. I., Sun, T., Zhao, J., Zhang, D., Yang, S., Liu, Z., Cheng, X., Terryn, H. and Li, X. (2021). Towards a better understanding of localised corrosion induced by typical non-metallic inclusions in low-alloy steels, *Corros. Sci.*, 179, 109150. DOI: 10.1016/j.corsci.2020.109150.
- [13] Wu, K., Jung, W. and Byeon, J. (2016). In-situ monitoring of pitting corrosion on vertically positioned 304 stainless steel by analyzing acoustic-emission energy parameter, *Corros. Sci.*, 105, pp. 8–16. DOI: 10.1016/j.corsci.2015.12.010.
- [14] Fabas, A., Monceau, D., Doublet, S. and Put, A.R.V. (2015). Modelling of the kinetics of pitting corrosion by metal dusting, *Corros. Sci.*, 98, pp. 592–604. DOI: 10.1016/j.corsci.2015.05.061.
- [15] Natesan, K. and Zeng, Z. (2007). Development of Materials Resistant to Metal Dusting Degradation, report ANL-07/30, Argonne National Laboratory, pp. 161.
- [16] Yu, J., Wang, H., Yu, Y., Luo, Z., Liu, W. and Wang, C. (2018). Corrosion behavior of X65 pipeline steel: Comparison of wet–Dry cycle and full immersion, *Corros. Sci.*, 133, pp. 276–287. DOI: 10.1016/j.corsci.2018.01.007.
- [17] Wang, Y., Xu, S. and Li, A. (2020). Flexural performance evaluation of corroded steel beams based on 3D corrosion morphology, *Struct. Infrastruct. E.*, 16(11), pp. 1562–1577. DOI: 10.1080/15732479.2020.1713169.
- [18] Cerit, M. (2019). Corrosion pit-induced stress concentration in spherical pressure vessel, *Thin Wall. Struct.*, 136, pp. 106–112. DOI: 10.1016/j.tws.2018.12.014.
- [19] Nakai, T., Matsushita, H., Yamamoto, N. and Arai, H. (2004). Effect of pitting corrosion on local strength of hold frames of bulk carriers (1st report), *Mar. Struct.*, 17(5), pp. 403–432. DOI: 10.1016/j.marstruc.2004.10.001.
- [20] Ok, D., Pu, Y. and Incecik, A. (2007). Computation of ultimate strength of locally corroded unstiffened plates under uniaxial compression, *Mar. Struct.*, 20(1-2), pp. 100–114. DOI: 10.1016/j.marstruc.2007.02.003.
- [21] Khedmati, M.R. and Nouri, Z.H.M.E. (2015). Analytical simulation of nonlinear elastic–plastic average stress–average strain relationships for un-corroded/both-sides randomly corroded steel plates under uniaxial compression, *Thin Wall. Struct.*, 86, pp. 132–141. DOI: 10.1016/j.tws.2014.10.012.
- [22] Cerit, M. (2013). Numerical investigation on torsional stress concentration factor at the semi elliptical corrosion pit, *Corros. Sci.*, 67, pp. 225–232. DOI: 10.1016/j.corsci.2012.10.028.
- [23] Zhang, S. and Zhou, W. (2020). Assessment of effects of idealized defect shape and width on the burst capacity of corroded pipelines, *Thin Wall. Struct.*, 154, 106806. DOI: 10.1016/j.tws.2020.106806.
- [24] Vansovich, K., Aistov, I. and Nakhlestkin, A. (2019). Application of a discrete model of fatigue defect growth for assessment of the safe operation life of the main pipeline section with a corrosion defect, In: IOP Conference Series: Materials Science and Engineering, IOP Publishing, 684(1), 012006. DOI: 10.1088/1757-899X/684/1/012006.
- [25] Sultana, S., Wang, Y., Sobey, A.J., Wharton, J.A. and Sheno, R.A. (2015). Influence of corrosion on the ultimate compressive strength of steel plates and stiffened panels, *Thin Wall. Struct.*, 96, pp. 95–104. DOI: 10.1016/j.tws.2015.08.006.
- [26] Huang, Y., Zhang, Y., Liu, G. and Zhang, Q. (2010). Ultimate strength assessment of hull structural plate with pitting corrosion damage under biaxial compression, *Ocean Eng.*, 37(17–18), pp. 1503–1512. DOI: 10.1016/j.oceaneng.2010.08.001.
- [27] Zhao, Z., Zhang, H., Xian, L. and Liu, H. (2020). Tensile strength of Q345 steel with random pitting corrosion based on numerical analysis, *Thin Wall. Struct.*, 148, 106579. DOI: 10.1016/j.tws.2019.106579.



- [28] Liang, Z., Xiao, Y. and Zhang, J. (2018). Stress–Strain Analysis of a Pipeline with Inner and Outer Corrosion Defects, *J. Press. Vess.-T.*, 140(6), 064501. DOI: 10.1115/1.4041434.
- [29] Wang, R., Guo, H. and Shenoi, R.A. (2020). Experimental and numerical study of localized pitting effect on compressive behavior of tubular members, *Mar. Struct.*, 72, 102784. DOI: 10.1016/j.marstruc.2020.102784.
- [30] Feng, L., Hu, L., Chen, X. and Shi, H. (2020). A parametric study on effects of pitting corrosion on stiffened panels' ultimate strength, *Int. J. Nav. Arch. Ocean*, 12, pp. 699–710. DOI: 10.1016/j.ijnaoe.2020.08.001.
- [31] Tee, K.F. and Wordu, A.H. (2020). Burst strength analysis of pressurized steel pipelines with corrosion and gouge defects, *Eng. Fail. Anal.*, 108, 104347. DOI: 10.1016/j.engfailanal.2019.104347.
- [32] Gao, J., Yang, P., Li, X., Zhou, J. and Liu, J. (2019). Analytical prediction of failure pressure for pipeline with long corrosion defect, *Ocean Eng.*, 191, 106497. DOI: 10.1016/j.oceaneng.2019.106497.
- [33] Zhang, Y., Huang, Y., Zhang, Q. and Liu, G. (2016). Ultimate strength of hull structural plate with pitting corrosion damage under combined loading, *Ocean Eng.*, 116, pp. 273–285. DOI: 10.1016/j.oceaneng.2016.02.039.
- [34] Mechab, B., Malika, M., Salem, M. and Boualem, S. (2020). Probabilistic elastic-plastic fracture mechanics analysis of propagation of cracks in pipes under internal pressure, *Frattura ed Integrità Strutturale*, 14(54), pp. 202–210. DOI: 10.3221/IGF-ESIS.54.15.
- [35] Vakaeva, A.B., Shuvalov, G.M. and Kostyrko, S.A. (2021). Interfacial stresses in bimaterial composites with nanosized interface relief, In: 8th International Conference on Computational Methods for Coupled Problems in Science and Engineering, COUPLED PROBLEMS 2019, pp. 679–688.
- [36] Ahmed, A.B., Houria, M.I., Fathallah, R. and Sidhom, H. (2019). The effect of interacting defects on the HCF behavior of Al-Si-Mg aluminum alloys, *J. Alloy. Compd.*, 779, pp. 618–629. DOI: 10.1016/j.jallcom.2018.11.282.
- [37] Lakhdari, A.A., Bubnov, S.A., Seddak, A., Ovchinnikov, I.I. and Ovchinnikov, I.G. (2020). Finite Element Modeling of the behavior of a hollow cylinder in a hydrogen-containing environment, *Frattura ed Integrità Strutturale*, 51, pp. 236–253. DOI: 10.3221/IGF-ESIS.51.19.
- [38] Sedova, O.S., Khaknazarova, L.A. and Pronina, Y.G. (2014). Stress concentration near the corrosion pit on the outer surface of a thick spherical member, In: IEEE 10th International Vacuum Electron Sources Conference, IVESC 2014, pp. 245–246. DOI: 10.1109/IVESC.2014.6892074.
- [39] Liao, Y., Liu, C., Wang, T., Xu, T., Zhang, J. and Ge, L. (2021). Mechanical behavior analysis of gas pipeline with defects under lateral landslide. *Proceedings of the Institution of Mechanical Engineers, Part C: Journal of Mechanical Engineering Science*, 235(23), pp. 6752–6766. DOI: 10.1177/09544062211017161.
- [40] Kostyrko, S., Grekov, M. and Altenbach, H. (2021). Coupled effect of curved surface and interface on stress state of wrinkled thin film coating at the nanoscale. *ZAMM Zeitschrift Fur Angewandte Mathematik Und Mechanik*. DOI: 10.1002/zamm.202000202.
- [41] Abakarov A., Pronina Y. and Kachanov M. (2022). Symmetric arrangements of cracks with perturbed symmetry: extremal properties of perturbed configurations, *Int. J. Eng. Sci.*, 171(4), 103617. DOI: 10.1016/j.ijengsci.2021.103617.
- [42] Carpinteri, A., Brighenti, R. and Vantadori, S. (2006). Notched shells with surface cracks under complex loading. *Int. J. Mech. Sci.*, 48(6), pp. 638–649. DOI: 10.1016/j.ijmecsci.2006.01.004.
- [43] Carpinteri, A., Brighenti, R. and Vantadori, S. (2009). Notched double-curvature shells with cracks under pulsating internal pressure, *Int. J. Pres. Ves. Pip.*, 86(7), pp. 443–453. DOI: 10.1016/j.ijpvp.2008.12.007.
- [44] Vaziri, A., Nayeb-Hashemi, H. and Estekanchi, H.E. (2002). Dynamic Response of Cracked Cylindrical Shells With Internal Pressure. *Proceedings of the ASME 2002 International Mechanical Engineering Congress and Exposition. Design Engineering*. New Orleans, Louisiana, USA, pp. 257–265. DOI: 10.1115/IMECE2002-33582.
- [45] Zhu, Y., Zhang, J., Yu, J., Zhou, X., Zhao, X., Yin, B., Tang, W. (2020). Buckling of externally pressurized corroded spherical shells with wall-thickness reduction in local region. *Int. J. Pres. Ves. Pip.*, 188, p. 104231. DOI: 10.1016/j.ijpvp.2020.104231.
- [46] Sedova, O.S. (2020). Stress calculation for a hollow sphere with inner surface defects, *Vector of Togliatti State University*, 2, pp. 68–73. In Russian. DOI: 10.18323/2073-5073-2020-2-68-73.
- [47] Zhu, Y., Guan, W., Wang, H., Zhao, M. and Zhang, J. (2021). Buckling of spherical shells with pitting corrosion under external pressure, *Ships Offshore Struct.*, pp. 1–10. DOI: 10.1080/17445302.2021.2000266.
- [48] Zhao, Z., Zhang, P., Zhou, S. and Fan, X. (2022). Collapse pressure of randomly corroded spherical shell, *Ocean Eng.*, 246, 110604. DOI: 10.1016/j.oceaneng.2022.110604.
- [49] Okulova, D. D., Sedova, O. S. and Pronina, Y. G. (2021). The Effect of Surface Defects Interaction on the Strength of a Pressurised Spherical Shell. *Procedia Structural Integrity*, 33, pp. 1055–1064. DOI: 10.1016/j.prostr.2021.10.117.
- [50] Sedova, O. S. (2020). Calculation of Stresses in a Spherical Shell with Internal Surface Defects. *Science Vector of Togliatti State University*, 2, pp. 68–73. DOI: 10.18323/2073-5073-2020-2-68-73.